Eur. Phys. J. B (2015) 88: 193
DOI: 10.1140/epjb/e2015-60011-0

THE EUROPEAN PHYSICAL JOURNAL B

Regular Article

Bayesian inference of interaction properties of noisy dynamical systems with time-varying coupling: capabilities and limitations

Jens Wilting[1,2,a,b] and Klaus Lehnertz[1,2,3]

[1] Department of Epileptology, University of Bonn, Sigmund-Freud-Straße 25, 53105 Bonn, Germany
[2] Helmholtz Institute for Radiation and Nuclear Physics, University of Bonn, Nussallee 14-16, 53115 Bonn, Germany
[3] Interdisciplinary Center for Complex Systems, University of Bonn, Brühler Straße 7, 53175 Bonn, Germany

Received 6 January 2015 / Received in final form 27 March 2015
Published online 3 August 2015 – © EDP Sciences, Società Italiana di Fisica, Springer-Verlag 2015

Abstract. We investigate a recently published analysis framework based on Bayesian inference for the time-resolved characterization of interaction properties of noisy, coupled dynamical systems. It promises wide applicability and a better time resolution than well-established methods. At the example of representative model systems, we show that the analysis framework has the same weaknesses as previous methods, particularly when investigating interacting, structurally different non-linear oscillators. We also inspect the tracking of time-varying interaction properties and propose a further modification of the algorithm, which improves the reliability of obtained results. We exemplarily investigate the suitability of this algorithm to infer strength and direction of interactions between various regions of the human brain during an epileptic seizure. Within the limitations of the applicability of this analysis tool, we show that the modified algorithm indeed allows a better time resolution through Bayesian inference when compared to previous methods based on least square fits.

1 Introduction

When investigating the dynamics of spatially extended systems, a division into smaller, largely autonomous but weakly interacting subunits has proven to be a fruitful approach in order to understand the whole system. If oscillating systems are coupled, their dynamics may synchronize towards a coherent collective behavior, which is observed in a variety of disciplines, ranging from physics to the neurosciences [1–19]. In order to understand such collective behavior, an as precise as possible characterization of the underlying coupling between the dynamical units is desirable, and usually targeted utilizing linear [20] and non-linear [21] time series analysis techniques. In general, such techniques aim at distinguishing between *strength* and *direction* of bivariate interactions or couplings. Following linear dependency methods such as Granger causality [22,23], more recent work on chaotic non-linear dynamics [24] focuses on different approaches such as information-theoretic ones [25], the Fokker-Planck formalism [26], recurrence in state space [27], or phase synchronization [6]. Most of these analysis techniques require the investigated systems to be stationary, but many systems experience evolving, transient, or short-term interactions. Addressing this issue, modifications and extensions of techniques had been proposed that aim at a characterization of transient couplings [28–34].

Recently, Stankovski et al. [35] proposed an analysis framework for the time-resolved characterization of interaction properties of noisy, coupled dynamical systems. Assuming gradual changes of the system dynamics, and based on the notion of phase increments [36], the framework uses Bayesian inference and knowledge propagation [37] between consecutive segments (or windows) of data. The inclusion of data from previous segments is supposed to allow for shorter window lengths without violating the requirement of a sufficiently densely sampled state space, thus enabling the tracking of more rapid and short-lived changes of interaction properties. It is claimed, that this framework is capable of inferring strength, directionality, and functional relation of the interaction of coupled dynamical systems, while being robust to the influence of noise.

Here, we examine the performance of this Bayesian inference framework with respect to these claims. Specifically, both its capacity and limitations are characterized with respect to the inference of interaction properties of structurally different coupled dynamical systems under conditions that mimic those when investigating empirical data. The framework is then used to estimate the temporal variation of interaction properties between different regions of the human brain during an epileptic seizure.

[a] *Present address:* Max-Planck-Institute for Dynamics and Self-Organization, Am Faßberg 17, 37077 Göttingen, Germany
[b] e-mail: jwilting@nld.ds.mpg.de

2 Method

Consider a population of L dynamical systems, which are assumed to be oscillatory and weakly coupled. If these oscillations are on a limit-cycle, the individual dynamics of each system can be expressed in terms of phase dynamics [2,3,38,39], which may still be possible approximatively for some non-linear and chaotic systems [40]. In this view, the state of each oscillator is defined through its phase ϕ_i, and the evolution equation of the oscillator population is given by:

$$\dot{\phi}_i = \omega_i + f_i(\phi_i) + \sum_{i \neq j} g_{ij}(\phi_i, \phi_j) + \xi_i \tag{1}$$

with the natural frequencies ω_i of the oscillators and coupling functions g_{ij} from oscillator j to i. The noise terms ξ_i are assumed Gaussian, i.e., $\langle \xi_i(t)\xi_j(\tau)\rangle = \delta(t-\tau)\, E_{ij}$, where the symmetric matrix $\mathbf{E}$ with elements E_{ij} encodes spatial correlations between the noise processes.

Given an oscillator population, time series $\phi_{i,n} = \phi_i(t_n)$ at discrete times $t_n = t_0 + nh$ with a timestep h between two samples and $n = 1, \ldots, N$ are observed experimentally. One important endeavor in order to gain insight about the individual and collective behavior is the inference of the natural frequencies ω_i, and the functions f_i and g_{ij}, which in principle determine the dynamical properties of the oscillators. Estimating the noise intensities ξ_i and spatial correlations may provide valuable additional information about the system and about possible external inputs. Assume that f_i and g_{ij} can be approximated by a finite set of appropriate basis functions $\Phi_{i,k}(\phi_1, \ldots, \phi_L)$, such that equation (1) can be rewritten as:

$$\dot{\phi}_i = \sum_{k=0}^{K} c_k^{(i)} \Phi_{i,k}(\phi_1, \ldots, \phi_L) + \xi_i \tag{2}$$

where $\Phi_{i,0} = 1$, $c_0^{(i)} = \omega_i$ and the rest of the $\Phi_{i,k}$ are a number of K basis functions with respective coefficients $c_k^{(i)}$ capable of adequately describing the coupling functions. In principle, this holds for nonlinear couplings, provided the functional basis reproduces the coupling mechanism. The task of inferring the interaction properties of the oscillators is reduced to the inference of these coefficients. We here use a set of functions $\sin(l\phi_1 - m\phi_2)$ and $\cos(l\phi_1 - m\phi_2)$ with $m = \pm 1$ for $l = 1$, $m \leq 3$ for $l = 0$, and $m = 0$ for $l \leq 3$, yielding 17 Fourier basis functions in total. This is the same functional basis used in reference [41]. Although references [35,42] use a decomposition into Fourier modes as well, it is not stated which modes exactly they include.

While a similar approach has already been taken before [41,43–45] using least square fits for estimating the model coefficients, Stankovski et al. [35,42] presented a method based on Bayesian inference, which is derived in references [35,42,46–51]. Let the experimental data be given in the form of a multivariate, L-dimensional time series $\mathcal{X} = \{\phi_{i,n} \equiv \phi_i(t_n)\}$, while the model parameters $\mathcal{M} = \{c_k^{(l)}, E_{ij}\}$ are to be inferred. If h is sufficiently small, the mid-point Euler discretization scheme

$$\dot{\phi}_{i,n} = \frac{\phi_{i,n+1} - \phi_{i,n}}{h}, \quad \phi^*_{i,n} = \frac{\phi_{i,n+1} + \phi_{i,n}}{2} \tag{3}$$

is used to describe the dynamics in terms of the observed discrete time series.

Assume that the model parameters are distributed with a certain probability density $\mathcal{P}_{\text{prior}}(\mathcal{M})$ which encloses prior knowledge. Given observational data $\mathcal{X}$, Bayes' theorem allows a refinement of the model parameters with respect to these data:

$$\mathcal{P}_{\mathcal{X}}(\mathcal{M}|\mathcal{X}) = \frac{\ell(\mathcal{X}|\mathcal{M})\, \mathcal{P}_{\text{prior}}(\mathcal{M})}{\int \ell(\mathcal{X}|\mathcal{M})\, \mathcal{P}_{\text{prior}}(\mathcal{M})\, d\mathcal{M}}. \tag{4}$$

The likelihood function $\ell(\mathcal{X}|\mathcal{M})$ is the probability to observe the data $\mathcal{X}$ for given prior model parameters $\mathcal{M}$. Thus Bayesian inference assigns a high probability to parameters which make the observed data likely, while suppressing parameters for which this is not the case. With known prior density the sole problem that remains is the calculation of the likelihood function, which can be performed analytically [46–51] under the restriction to white noise.

If the prior density is Gaussian, the posterior will be Gaussian again. A two-step iteration scheme [42] yields the most probable values for the coefficients in equation (2):

$$\begin{aligned}
E_{ij} &= \sum_{n=0}^{N-1} \frac{h}{N} \left(\dot{\phi}_{i,n} - \sum_{k=0}^{K} c_k^{(i)} \Phi_{i,k}(\phi^*_{\cdot,n}) \right) \\
&\quad \times \left(\dot{\phi}_{j,n} - \sum_{k=0}^{K} c_k^{(j)} \Phi_{j,k}(\phi^*_{\cdot,n}) \right), \\
\Xi^{(i,j)}_{kw} &= (\Xi_{\text{prior}})^{(i,l)}_{kw} + h \sum_{n=0}^{N-1} \Phi_{i,k}(\phi^*_{\cdot,n})(E^{-1})_{ij} \Phi_{j,w}(\phi^*_{\cdot,n}), \\
r_k^{(i)} &= \sum_{l=1}^{L} \sum_{w=0}^{K} \left(\Xi^{-1}_{\text{prior}} \right)^{(i,l)}_{kw} c_w^{(l)} \\
&\quad + h \sum_{n=0}^{N-1} \sum_{l=1}^{L} \left[\Phi_{i,k}(\phi^*_{\cdot,n})(E^{-1})_{il} \dot{\phi}_{l,n} - \frac{1}{2} \frac{\partial \Phi_{l,k}(\phi_{\cdot,n})}{\partial \phi_l} \right], \\
c_k^{(i)} &= \sum_{l=1}^{L} \sum_{w=0}^{K} \left(\Xi^{-1} \right)^{(i,l)}_{kw} r_w^{(l)},
\end{aligned} \tag{5}$$

that give estimators E_{ij} for the noise correlation matrix and $\Xi^{(i,j)}_{kw}$ for the inverse covariance matrix of the Gaussian posterior density $\mathcal{P}_{\mathcal{X}}$. The $c_k^{(i)}$ are the most probable coefficient values under this probability density.

Given a prior density $\mathcal{P}_{\text{prior}}(\mathcal{M})$, equations (5) yield the posterior distribution $\mathcal{P}_{\mathcal{X}}$. If the experimental data consist of a stream of data, where the time series is divided into B smaller windows, the posterior of one window can be used as a prior for the subsequent one. This way, the knowledge becomes more and more refined as more data are taken into account.

However, this approach is too restrictive if the inferred parameters are subject to changes over time, as a sharply peaked Gaussian prior distribution allows very little variability away from the most probable value of $\mathcal{P}_{\text{prior}}(\mathcal{M})$. This problem is tackled by broadening the posterior density of one window, so that the prior density for the next window allows changes away from this most probable value. This broadening is implemented by adding a matrix $\hat{\mathbf{\Sigma}}_{\text{diff}}$, which effectively implements a normal diffusion of the parameter probabilities:

$$\hat{\mathbf{\Sigma}}^{b+1}_{\text{prior}} = \hat{\mathbf{\Sigma}}^{b}_{\text{post}} + \hat{\mathbf{\Sigma}}^{b}_{\text{diff}}. \tag{6}$$

In principle, the diffusion matrix takes a form $(\Sigma_{\text{diff}})_{ij} = \rho_{ij}\sigma_i\sigma_j$ with standard deviations σ_i of the diffusion of the coefficients c_i, but assume here that the changes of the parameters are uncorrelated and the matrix is diagonal, i.e., $\rho_{ij} = \delta_{ij}$.

Originally [35,42], σ_i were estimated as a fixed fraction of the parameter values, $\sigma_i = p_w\, c_i$. The parameter p_w governs how much prior information is lost and has to be chosen appropriately. However, we will demonstrate that this method inevitably yields biased inference results, and propose a modified approach: Assume, that the parameters values c_i^b are known for each window b. Then, the change from one window to the next one can be estimated by:

$$\sigma_i^b = c_i^{b+1} - c_i^b. \tag{7}$$

With these estimators for the probability diffusion, and starting from the first window, the inference is repeated. According to equation (6) this choice of σ_i^b always ensures, that the most probable value of c_i^{b+1} from the *previous* iteration is within one standard deviation of the most probable value of c_i^b in the *next* iteration. This algorithm gradually adapts the σ_i^b such that enough variability is allowed to track changing parameters where necessary, while making best use of knowledge propagation where possible. Of course, as knowledge about the parameter values for all windows is required, this modification is only applicable in offline data analysis.

2.1 Estimation of interaction properties

Based upon the inferred coefficients $c_k^{(i)}$, the following estimators are used for the characterization of interacting properties:

1. The natural frequencies are inferred by $\hat{\omega}_i = c_0^{(i)}$.
2. Let $\kappa = \{k : \partial\Phi_k^{(i,j)}/\partial\phi_j \neq 0\}$ be the set of indices, where the basis function describing the dynamics of oscillator i depends upon ϕ_j (i.e., is part of the coupling from j to i). The coupling strength from oscillator j onto oscillator i is characterized by the norm of the coefficient vector $(c_k^{(i)})_{k\in\kappa}$,

$$\hat{K}_{j\to i} = \sqrt{\sum_{k\in\kappa}\left(c_k^{(i)}\right)^2}. \tag{8}$$

3. The direction of the interaction is characterized by:

$$\hat{d}^{j\to i} = \frac{\hat{K}_{j\to i} - \hat{K}_{i\to j}}{\hat{K}_{j\to i} + \hat{K}_{i\to j}} \tag{9}$$

and takes values around 0 if there is no or equally strong coupling, and values around ± 1 if the interaction is completely directed.

We compare the directionality inferred by the Bayesian inference method to the directionality index $\hat{d}^{j\to i}_{\text{EMA}}$ obtained with the well-established evolution map approach [41] (EMA). With EMA, the same approximation (2) of the system dynamics is used, but the optimal coefficients are estimated with a least square method.

Coupling strength estimation is compared to the mean phase coherence [52]

$$R = \left|\frac{1}{N}\sum_{n=1}^{N-1} e^{i(\phi_{1,n}-\phi_{2,n})}\right|, \tag{10}$$

which is a measure of phase locking, with $R = 0$ indicating no synchronization at all and $R = 1$ meaning perfect phase coherence.

2.2 Non-linear model systems with constant coupling

The capability of the method in inferring interaction properties of phase oscillators and Poincaré oscillators, which are limit cycle systems, has been shown before [35,42]. Here, we will investigate the method when applied to nonlinear systems with chaotic dynamics at the paradigmatic examples of Rössler and Lorenz systems.

The dynamics of two diffusively coupled noisy Rössler oscillators [53] obeys the equations

$$\begin{aligned}
\dot{x}_i^{\text{R}} &= \omega_i\,\left(-y_i^{\text{R}} - z_i^{\text{R}}\right) + K_{j\to i}\,\left(x_j^{\text{R}} - x_i^{\text{R}}\right) + \xi_x,\\
\dot{y}_i^{\text{R}} &= \omega_i\,\left(x_i^{\text{R}} + a y_i^{\text{R}}\right) + \xi_y,\\
\dot{z}_i^{\text{R}} &= \omega_i\,\left(b + z_i^{\text{R}}\,\left(x_i^{\text{R}} - c\right)\right) + \xi_z,
\end{aligned} \tag{11}$$

with $i \in \{1,2\}$, the parameter values $a = 0.15$, $b = 0.2$ and $c = 10.0$, and dynamical noise of varying intensity. In the presented setup the frequency of the oscillation can slightly be adjusted through ω_i.

Secondly, the Rössler oscillator defined by equation (11) is coupled diffusively to a Lorenz oscillator [54,55]

$$\begin{aligned}
\dot{x}^{\text{L}} &= \beta_1\,\left(y^{\text{L}} - x^{\text{L}}\right)\\
\dot{y}^{\text{L}} &= x^{\text{L}}\,\left(\beta_2 - z^{\text{L}}\right) - y^{\text{L}}\\
\dot{z}^{\text{L}} &= x^{\text{L}} y^{\text{L}} - \beta_3 z^{\text{L}} + K_{\text{R}\to\text{L}}\,\left(x^{\text{R}} - z^{\text{L}}\right)
\end{aligned} \tag{12}$$

with $\beta_1 = 10$, $\beta_2 = 28$ and $\beta_3 = 2.66$. The z-variable of the Lorenz dynamics allows a better (in contrast to the x and y variables) phase definition. Therefore, the Lorenz oscillator is also coupled in its z-component, while the Rössler oscillator is coupled through its x-component by

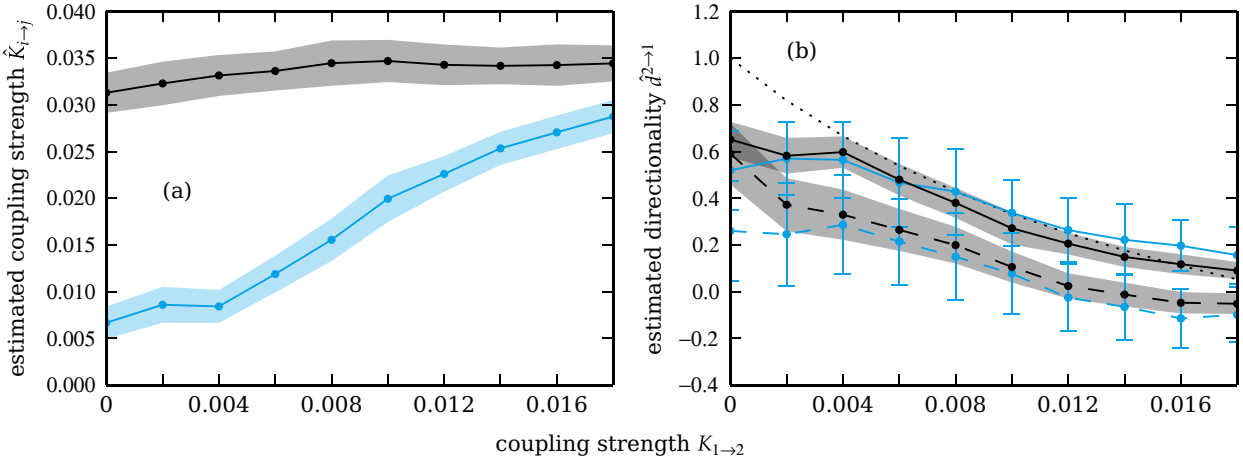

Fig. 1. (a) Estimated coupling strengths $\hat{K}_{2\to1}$ (black) and $\hat{K}_{1\to2}$ (blue) as a function of coupling strength $K_{1\to2}$. (b) Estimated directionality $\hat{d}^{2\to1}$ as a function of coupling strength $K_{1\to2}$, obtained by the Bayesian inference algorithm (black) and the EMA method (blue), for two coupled Rössler oscillators with $\omega_1 = 0.9$, $\omega_2 = 1.1$ (solid lines) and $\omega_1 = 1.1$, $\omega_2 = 0.9$ (dashed lines). Estimated directionality should lie on the dotted line. Averages and standard deviations (shaded areas or error bars) over 100 independent realizations are shown.

neglecting the lower indices i and j in equation (11) and replacing x^{R} by z^{L} with the parameters chosen as before except for $\omega_i = 2.0$.

The systems are integrated numerically with Conedy [56] using an Euler scheme for stochastic differential equations when dynamical noise is present in the system and with a fourth order Runge-Kutta method otherwise. The integration step size is 0.01, and the sampling step is $h = 0.2$. In order to avoid transient effects, the simulation is run for 100 time units first and is only then observed recording the dynamical variables x_i^{R} and z^{L} until 61440 data points (corresponding to 15 windows of length 4096) are sampled. We generate 100 realizations of the systems by randomly choosing the initial conditions in state space near the attractors.

Phase information are obtained as $\arctan \frac{\mathcal{H}\{x\}(t)}{x(t)}$ by applying the Hilbert transform [57]

$$\mathcal{H}\{x\}(t) = \frac{1}{\pi}\mathrm{p.v.}\int_{-\infty}^{\infty}\frac{x(\tau)}{t-\tau}d\tau \qquad (13)$$

with the Cauchy principal value p.v. to the recorded dynamical observables in order to mimic realistic conditions of analysis.

2.3 Model systems with time-varying coupling

To investigate systems, where the coupling strengths are not constant any more but are subject to changes over time, we use a pair of coupled noisy phase oscillators

$$\dot{\phi}_i(t) = \omega_i + K_{j\to i}(t)\,\sin\left(\phi_j(t) - \phi_i(t)\right) + \xi_i(t). \qquad (14)$$

The coupling strengths $K_{j\to i}$ are functions of time due to an external forcing. The exact correspondence of the model parameters to the inferred coefficients allows quantification of the goodness of inference results (see Sect. 4).

The natural frequencies are fixed at $\omega_1 = 1.1$ and $\omega_2 = 0.9$, and the noise amplitude is chosen at $\xi_i = 0.1$ for both oscillators. An Euler integration scheme with step-width 0.01 is used for numerical integration. The noise is included by drawing a normally distributed random variable $\xi_{i,n} \sim \mathcal{N}(0, h\,\xi_i^2)$ in each step. Transient behavior of the system is discarded by omitting the first 10 000 steps of integration. After that, the simulation is run recording every 20th step, yielding a sampling width of $h = 0.2$, until $B\,N$ values of the observables $\phi_{1,2}$, corresponding to B windows of length N, are recorded. Every simulation is repeated 100 times with initial conditions $\phi_1(0)$, $\phi_2(0)$ drawn randomly from a uniform distribution on $[0, 2\pi)$.

3 Investigation of model systems with time-independent couplings

3.1 Coupled Rössler oscillators

Consider two Rössler oscillators according to equation (11), which are structurally identical up to slightly different natural frequencies ($\omega_1 = 0.9$ and $\omega_2 = 1.1$). The coupling strengths are kept constant during every simulation, but between simulations $K_{1\to2}$ is varied from 0 to 0.02, while $K_{2\to1} = 0.02$ always. For every set of parameters, inference is applied to 100 independent realizations of the system dynamics with randomly chosen initial conditions. We infer coupling strengths using the Bayesian framework, and coupling directions both with the Bayesian and the conventional EMA approach. The inference results are presented in Figure 1. The estimated coupling strengths reflect the changes of the underlying coupling strengths, with $\hat{K}_{2\to1}$ being constant and $\hat{K}_{1\to2}$ increasing monotonously.

We find that, if $K_{1\to 2} = 0$, this coupling strength is slightly overestimated by the Bayesian inference method with $\hat{K}_{1\to 2} \approx 0.007$. This rather small deviation from 0 has a more obvious effect upon the estimation of coupling direction: in the case of directed couplings it leads to an underestimation of the directionality by $\hat{d}^{2\to 1} \approx 0.6$. Indeed we find that the smaller the number of basis functions (provided sufficient approximation of the phase dynamics), the smaller the bias of underestimating interaction direction. This result emphasizes the importance of finding an appropriate set of basis functions.

Generally, and particularly visible in bidirectional coupling $K_{1\to 2} = K_{2\to 1} = 0.02$, the directionality of the coupling is biased in favor of the faster oscillator, which is spuriously detected as a driving force even if the coupling is symmetric. This bias is slightly smaller for the investigated Rössler oscillator when using the Bayesian inference method, but nonetheless still apparent.

If white noise is coupled dynamically to the oscillator (we investigated signal-to-noise ratios between 2500 and 50, data not shown), we find that the general performance of both the Bayesian inference method and the conventional evolution map approach is decreased: while the bias of directionality towards the faster oscillator persists, the directional coupling is strongly underestimated by both estimators for $d^{2\to 1} = 1$, with Bayesian inference performing only slightly better ($\hat{d}^{2\to 1} < 0.15$) than EMA ($\hat{d}^{2\to 1}_{\mathrm{EMA}} < 0.08$).

3.2 Coupled Rössler and Lorenz oscillators

We also investigate the inference of interaction direction between two structurally different systems, whose individual attractors differ topologically, at the example of a Rössler oscillator coupled to a Lorenz oscillator according to equation (12). We switch off coupling in one direction completely ($K_{\mathrm{R}\to\mathrm{L}} = 0$ or $K_{\mathrm{L}\to\mathrm{R}} = 0$) and vary the coupling strength in the other direction ($K_{\mathrm{L}\to\mathrm{R}}$ or $K_{\mathrm{R}\to\mathrm{L}}$ respectively) between 0 and 1. Hence we expect the directionality $d^{\mathrm{R}\to\mathrm{L}} = 0$ if there is no coupling at all, $K_{\mathrm{L}\to\mathrm{R}} = K_{\mathrm{R}\to\mathrm{L}} = 0$, and in all other cases $d^{\mathrm{R}\to\mathrm{L}} = -1$ or $d^{\mathrm{R}\to\mathrm{L}} = 1$ respectively.

As depicted in Figure 2, directionality is not estimated correctly by either method. Even if there is no coupling present at all, $\hat{d}^{\mathrm{R}\to\mathrm{L}}_{\mathrm{Bayes}}$ and $\hat{d}^{\mathrm{R}\to\mathrm{L}}_{\mathrm{EMA}}$ take values around -0.5, suggesting directed interactions from the Lorenz to the Rössler oscillator. If $K_{\mathrm{L}\to\mathrm{R}} \approx 1$ or $K_{\mathrm{R}\to\mathrm{L}} \approx 1$, the Bayesian estimators at least show the correct sign of the directionality, while EMA suggests coupling in the opposite direction in both cases. However, if the Rössler oscillator drives the Lorenz oscillator (blue lines in Fig. 2), the direction of this interaction is estimated with the wrong sign up to values of $K_{\mathrm{R}\to\mathrm{L}} = 0.3$. In consequence, no reliable estimation of directionality is possible here.

Our studies with model systems show, that interaction properties can only be inferred with the Bayesian inference framework [35] if a phase-based description is meaningful. In non-linear systems with chaotic dynamics this is usually not the case. Structural differences (e.g. differing natural frequencies or topologically different attractors) between oscillators limit the applicability of the Bayesian inference method and lead to spurious results, similarly to many other methods as has been pointed out in previous studies [43,55,58–61].

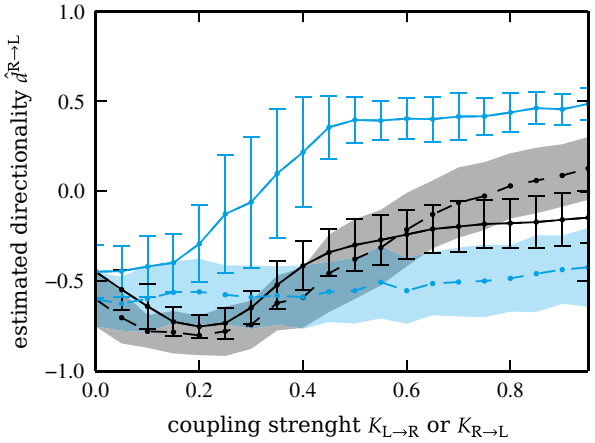

Fig. 2. Estimated directionality index $\hat{d}^{\mathrm{R}\to\mathrm{L}}$ as a function of coupling strength inferred with the Bayesian method (solid lines) and EMA (dashed lines), if $K_{\mathrm{R}\to\mathrm{L}}$ or $K_{\mathrm{L}\to\mathrm{R}}$ is kept zero, while $K_{\mathrm{L}\to\mathrm{R}}$ (black) or $K_{\mathrm{R}\to\mathrm{L}}$ (blue), respectively, is varied from 0 to 1. Averages and standard deviations (shaded areas or error bars) over 100 independent iterations are shown.

4 Investigation of time-evolving couplings

4.1 Influence of the choice of the parameter p_w

When investigating the time-dependence of interaction properties, prior knowledge must be neglected partially. In the original inference method [35] this forgetting is regulated through the parameter p_w (see Sect. 2). It has been shown before [35,42], that the choice of the parameter p_w influences the ability to track rapid changes of interaction properties. We examine this influence in more detail at the example of noisy phase oscillators (see Sect. 2.3) with different time-dependent changes of the coupling strength, which are depicted in the insets of Figures 3a–3f. We here chose to not investigate time-evolving non-linear systems in the light of the shortcomings in characterizing interactions between non-linear systems already in the stationary case. For every window b, the inference yields one set of coefficients $c_k^{(i),b}$. Let $\hat{\alpha}^b\left(\{c_k^{(i),b}\}_{k=0,\ldots K}^{i=1,\ldots,L}\right)$ be an estimator, which is a function of these coefficients (e.g., the estimators for direction and strength of interactions used here), and let α denote the corresponding "true" value, which is to be inferred. We generate time series with the original sampling width h by means of step functions, i.e.

$$\hat{\alpha}(t_j) = \sum_{b=0}^{B-1} \hat{\alpha}^b \, \chi_{\tau_b}(j) \qquad (15)$$

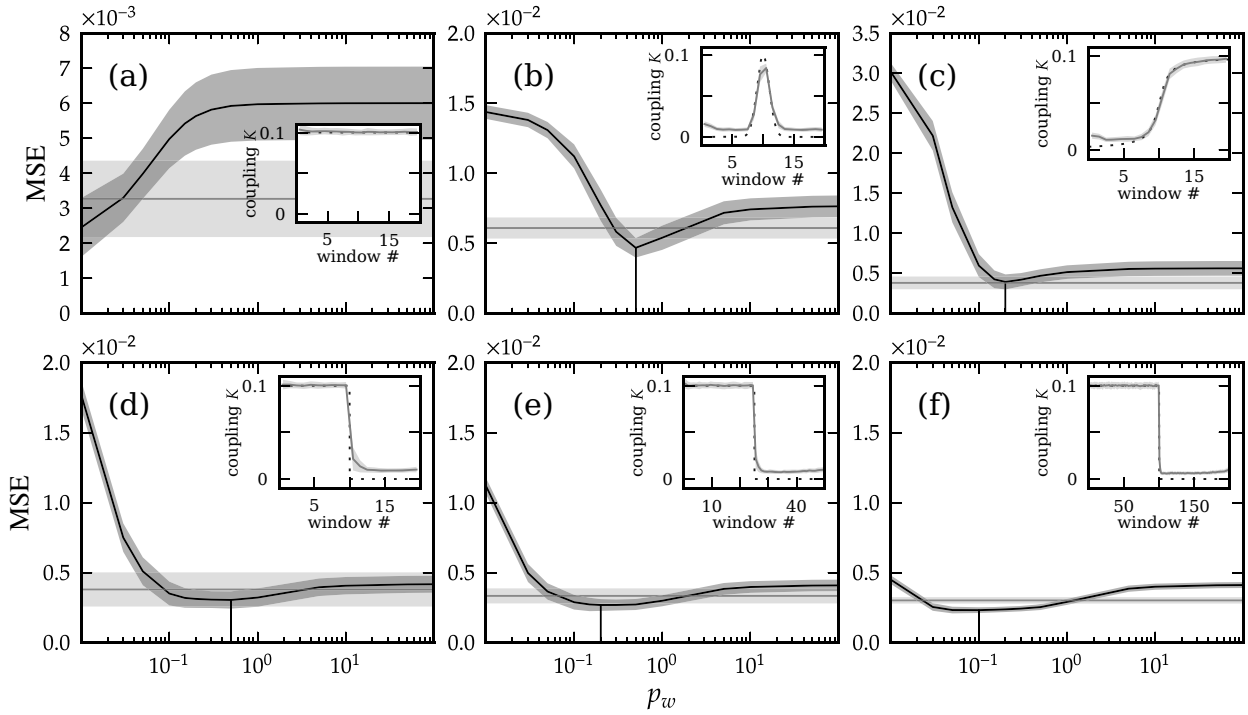

Fig. 3. The estimator $\mathrm{MSE}(\hat{K}_{2\to1}, K_{2\to1})$ for the goodness of the original inference algorithm [35] as a function of the choice of the parameter p_w (black vertical lines indicate optimal choice of p_w) for different time-dependent changes (parts (a)−(f)) of the coupling $K_{2\to1}(t)$. The MSE thresholds for the modified algorithm are indicated by gray horizontal lines. Averages and standard deviations (shaded areas) over 100 independent iterations are shown. Note the different scales of the MSEs. The insets show the coupling strength as a function of time (dotted lines), together with the time-resolved estimator of coupling strength $\hat{K}_{2\to1}$ inferred by the modified algorithm with a window length of 4096 (solid lines; for part (c), results from the original inference algorithm were shown in Ref. [42]). In parts (d)−(f), the coupling changes abruptly in the middle of the time series. Note that the time series differ in their lengths (20, 50, and 200 windows respectively), and hence have stationary periods of different durations.

where the set $\tau_b = \{b\,N, \ldots, (b+1)\,N-1\}$ denotes all time step indices that have been assigned to window b. These allow the calculation of the expected deviation of the inferred estimator from its reference value, even when the reference value changes on time scales smaller than one window length N.

The parameter p_w is varied from 10^{-2} to 10^2. We consider the mean squared error

$$\mathrm{MSE}\,(\hat{\alpha}, \alpha) = \frac{1}{T}\int_0^T \left(\hat{\alpha}(t) - \alpha(t)\right)^2 dt \qquad (16)$$

and investigate the dependence of MSE upon the parameter p_w at the example of the coupling strength ($K_{2\to1}$ inferred by $\hat{K}_{2\to1}$). We find, that the optimal choice of p_w that minimizes $\mathrm{MSE}(\hat{K}_{2\to1}, K_{2\to1})$ depends upon the type of the underlying temporal variation of the coupling (see Fig. 3). In the case of constant coupling strength (Fig. 3a), it is at $p_w = 0$, but varies up to 0.5 in other cases (Figs. 3b and 3d).

We emphasize that there is *not* one globally optimal choice for p_w. Hence, knowledge about the outcome of the inference algorithm is required prior to applying it in order to ensure reliable performance of the method.

Apart from this challenge of appropriately choosing p_w, we stress an inherent bias in the inference algorithm: as prior knowledge is ignored proportionally to the value of the inferred coupling itself, $\sigma_i = p_w c_i$, a change from a high absolute value of c_i will always be more readily followed than a change from small c_i.

4.2 Modified algorithm for inferring time-evolving interaction properties

The proposed modification of the algorithm aims at resolving the described problems. We now use this modified algorithm to infer the same time-depending couplings investigated before.

The inferred evolution of the coupling strengths reflects the underlying time-varying coupling quite well (insets Fig. 3). The time dependent forgetting σ_i^b from equation (7), based upon the coupling strength differences between adjacent windows, is proportional to the temporal changes of the coupling and allows variability where needed while preserving knowledge propagation where possible, regardless of the current values of the estimated coupling. Estimating the necessary limitation of knowledge propagation in terms of the temporal changes

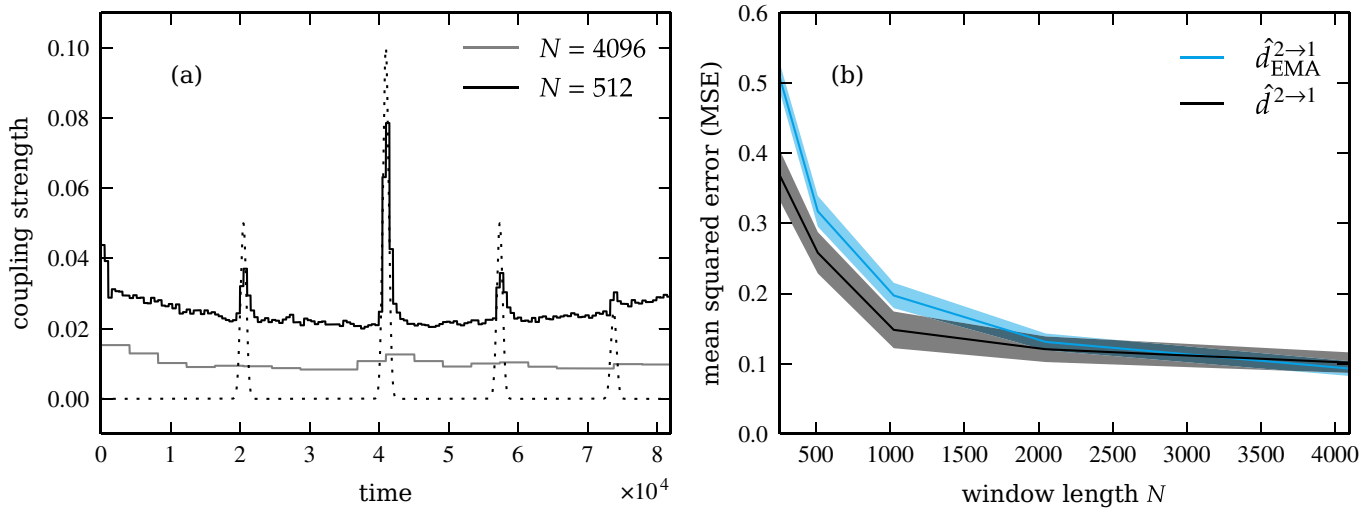

Fig. 4. (a) Exemplary evolution of the coupling strength $K_{2\to1}$ (dotted line) inferred by $\hat{K}_{2\to1}$ with window lengths $N = 4096$ (gray) and $N = 512$ (black). Why the bias increases at both ends of the time series remains open for future studies. (b) Mean squared error $\mathrm{MSE}(\hat{d}^{2\to1}, d^{2\to1})$, averaged over 100 independent iterations with standard deviations indicated by shaded areas, as a function of the window length N for our modified Bayesian inference (black) and the original EMA (blue) method. Findings obtained with the original Bayesian method are similar to those obtained using EMA for large p_w. For very small p_w, inference results do not resolve the short-lived peaks of the coupling strength, and for optimally chosen p_w they are similar to those obtained with our modified method (see [42] and Fig. 3).

of the coupling strengths instead of their current *values* themselves appears more appropriate as shown here.

The performance of this proposed inference algorithm is again characterized in terms of the MSE. As no parameter choice is required here, the achieved goodness is represented by global goodness thresholds in Figure 3. It is revealed, that for all inspected time courses of the coupling strengths (see insets of Fig. 3), the goodness of the original algorithm outperforms our modified method only for a small range of values of p_w. The width and position of this range, however, depend on the particular time course of the coupling strength. For a constant coupling strength (Fig. 3a) very large values of p_w, for time courses of the coupling strength that include variations (Figs. 3b–3f) very small values of p_w lead to a large increase of the MSE. Hence, particularly for field studies when the exact time course of the coupling strength is usually unknown, the optimal choice of p_w requires some fine-tuning. Interestingly, our modified algorithm performs close to the optimal p_w regardless of the couplings investigated here. Therefore, our algorithm is likely to yield more reliable results than the original one if no prior knowledge about the time-dependence of the inferred interactions is available, and does not impose the challenge of choosing a critically important parameter. Furthermore, it does not suffer from the bias outlined above.

On the downside, this modified algorithm has limited goodness when inferring constant interaction properties. Small parameter differences between adjacent windows tend to sustain themselves by limiting the extent of prior knowledge passed on to the next window, giving a non-vanishing limit upon the achievable goodness (note that this effect is also present in the original algorithm [35], where this limitation depends upon the estimated value of the coupling strength itself). It will have to be subject of future investigations if this effect can be suppressed.

4.3 Time resolution and goodness of inference

We compare the Bayesian inference method with the original evolution map approach [41] with respect to goodness (in terms of the MSE) of inferring time-dependent interaction properties as a function of the temporal resolution. Again, the phase oscillators defined in equation (14) are inspected as a model system.

A higher temporal resolution using smaller window length N, is favorable in order to reveal short-lived, transient changes of the interactions or to determine the timing of a change in the coupling. We demonstrate this at the example of short-lived Gaussian peaks of the coupling strength $K_{2\to1}$, which are on the time scale of 4096 data points.

As can be seen from Figure 4a, these short increases of coupling strength cannot be revealed if the window length is $N = 4096$, but if the temporal resolution is improved, the transient increases in coupling strength are detected indeed. On the downside, less data per window increase bias towards estimating finite coupling strength even if coupling is absent between the investigated systems. This bias does not surprise, given it arises from small deviations from 0 in a larger number of coefficients, and the partial suppression of knowledge propagation in the presented modification of the inference algorithm. Nevertheless, comparing the mean squared error $\mathrm{MSE}(\hat{K}_{2\to1}, K_{2\to1})$ for the presented algorithm with that

obtained by the original EMA method (Fig. 4b), (partial) knowledge propagation indeed helps to improve the goodness when reducing the window length N. Therefore, when the characterization of interactions is required with high temporal resolution, the use of our modified method is beneficial.

5 Estimating interaction properties in the human epileptic brain

Brain signals during an epileptic seizure exhibit oscillatory behavior with complex spatial and temporal changes in frequency content [62–65]. The identification of brain regions that are involved in the genesis, propagation and termination of seizures and the time-resolved characterization of strength and direction of interactions between these regions can help to advise new developments that aim to efficiently control seizures [66–72].

We here consider multichannel intracranial electroencephalographic (EEG) data of 5 min duration centered around a focal epileptic seizure that was recorded from an epilepsy patient undergoing presurgical evaluation. The patient had signed informed consent that her/his clinical data might be used and published for research purposes, and the study protocol had previously been approved by the local medical ethics committee. The EEG was recorded prior to surgery via two intrahippocampal depth electrodes (each equipped with 10 cylindrical contacts of length 2.5 mm and an intercontact distance of 4 mm; implanted stereotactically in the medial temporal lobes) and from grid electrodes (rectangular flexible grid of 8×4 contacts with an intercontact distance of 10 mm; placed subdurally onto the temporal lateral neocortex) referenced against the average activity of two recording contacts (GLA1 and GLA2) distant to the seizure-onset zone (SOZ covered by contact GLD6, Fig. 5a). Data were band-pass filtered between 0.1−70 Hz and sampled at 200 Hz using a 16 bit analog-to-digital converter. Prior to estimating strengths and direction of interactions, we digitally band-pass filtered the data between 1 and 45 Hz (2nd order Butterworth characteristic), suppressed possible contributions of the power line frequency using a notch filter, and derived phase time series via the Hilbert transform [52,57].

We divided the data into disjoint segments of 20.48 s duration (corresponding to 4096 data points) and estimated the direction of interaction $\hat{d}_{\mathrm{EMA}}$ using the EMA approach [41] and the strength of interaction using the mean phase coherence R [52]. These were compared to estimates of strength ($\hat{K}$) and direction ($\hat{d}$) of interaction obtained with our modification of the Bayesian inference approach (Sects. 2 and 4.2). For the latter, we considered segments of 20.48 s duration as well as shorter ones of 5.12 s (1024 data points) and 2.56 s (512 data points) duration benefiting from the better temporal resolution allowed by knowledge propagation. This analysis yields estimators for coupling strength and direction for each combination of pairs of recording contacts in a moving-window fashion.

We chose exemplary short- and long-ranged interaction between various brain regions: SOZ (GLD6) and its direct neighborhood (GLD7), SOZ and hippocampus of the opposite (contralateral) brain hemisphere (TR03), two adjacent intrahippocampal contacts (TR02, TR03), and two regions from the temporal lateral neocortex (GLD1, GLA8) spatially separated both from each other and from the SOZ. The findings for these brain regions are presented in Figure 5.

Bayesian inference unveiled a slight decrease in coupling strength $\hat{K}$ from the neighborhood of the SOZ to the SOZ itself (GLD6, GLD7, Fig. 5c) prior to the seizure, followed by a slight increase during the seizure. This did not reflect the increase of the mean phase coherence R at the onset of the seizure. Interestingly, the direction of interaction between these brain regions was estimated rather constant around 0 by both EMA and Bayesian inference (Fig. 5d). The small tendency towards identifying the neighboring brain area as driving the SOZ surprises, as the SOZ was *not* identified as the driving force here. Findings were consistent among all inspected windows lengths.

The strength of interactions between SOZ and the contralateral hippocampus (GLD6, TR03, Fig. 5e) estimated by Bayesian inference slightly decreased over the whole recorded time span, which did not explain the increase of R at the seizure onset. Both Bayesian inference and EMA identified the contralateral hippocampus to be driven by the SOZ most of the time (Fig. 5f), although there was a deviation between both directionality estimators at the end of the seizure. Again, results obtained by Bayesian inference were qualitatively consistent among all window lengths.

The two adjacent contacts within the contralateral hippocampus (TR02, TR03, Fig. 5g) were highly coherent over the whole recording period, as identified by $R \approx 1$ constantly for all windows. Hence, and conforming with numerical investigations on systems restricted to the synchronization manifold, the Bayesian estimators of the strength of interactions obtained from different window lengths differed, as no information on the whole phase space was available in order to reliably infer interaction properties. It is interesting to note, that the directionality was still inferred consistently over all windows lengths using Bayesian inference (Fig. 5h). However, it differed from the direction of interaction estimated by EMA, which indicated a reversal of the direction at seizure onset.

The interaction between two spatially separated areas from the temporal lateral neocortex (GLD1, GLA8) showed confounding evolution of both $\hat{K}$ and $\hat{d}$, where both strength and direction of interaction inferred by Bayesian inference differed significantly between different window lengths inspected (Figs. 5i and 5j). This phenomenon has not been observed in any of our numerical studies with model data before.

Overall, neither the improved time resolution nor the characterization of strength and direction of couplings

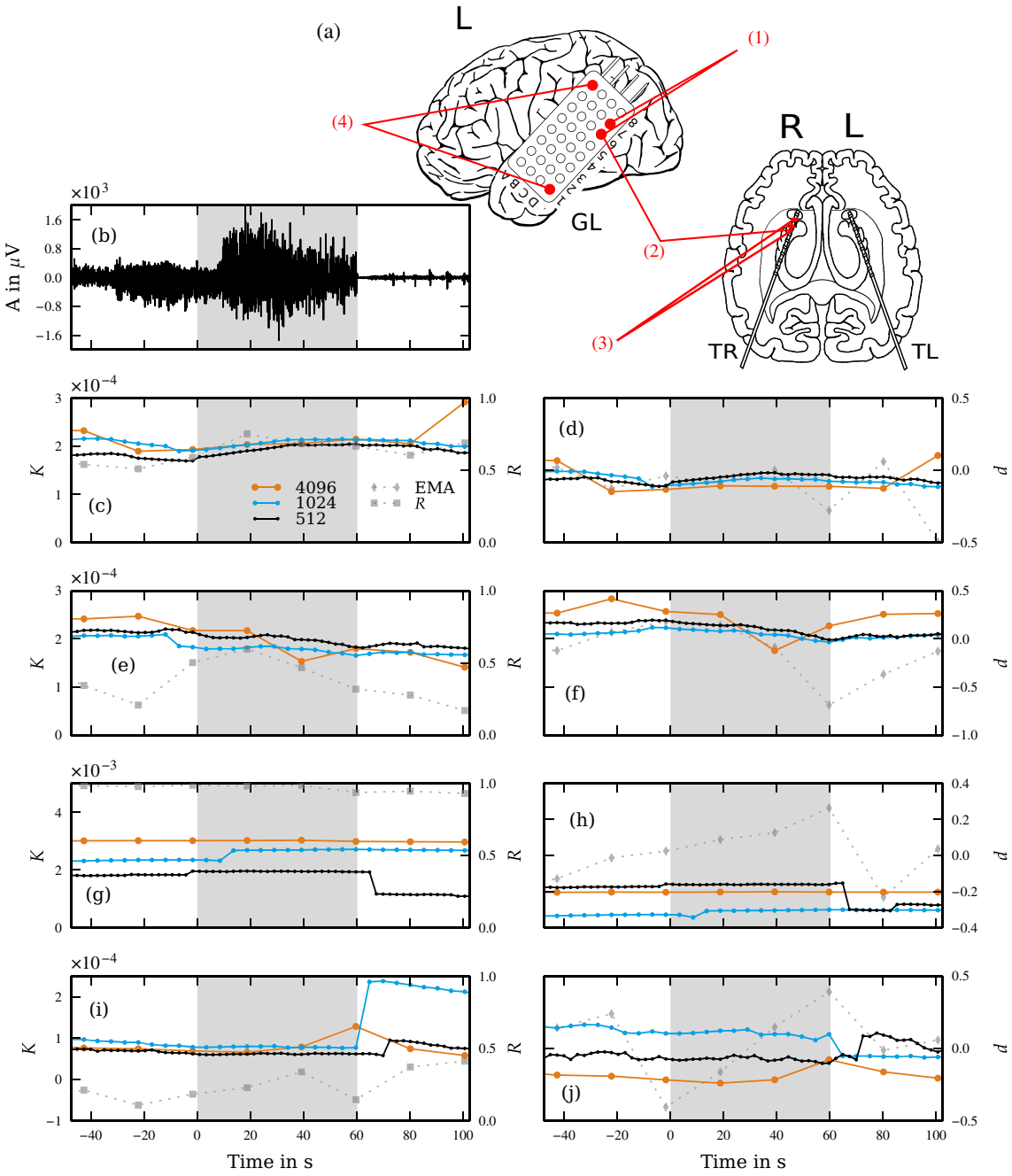

Fig. 5. (a) Schematics of the electrode grid placed over the left temporal lateral neocortex and the bilateral intrahippocampal depth electrodes. (b) EEG recording from GLD6 covering the seizure onset zone. (c)−(j) Estimators $\hat{K}$ and R for coupling strength (left), $\hat{d}_{\mathrm{EMA}}$ and $\hat{d}$ for interaction direction (right) from electrode pairs (GLD7, GLD6), (TR03, GLD6), (TR02, TR03), and (GLD1, GLA8) per line from top to bottom, see (1) to (4) in (a). The gray-shaded area indicates the seizure, and time points refer to the beginning of a window. R and $\hat{d}_{\mathrm{EMA}}$ are shown for a window length of 4096 data points, Bayesian results $\hat{K}$ and $\hat{d}$ also for shorter windows of length 1024 and 512.

does reveal any transient changes of the interaction properties of different brain areas that can help identifying beginning and end of an epileptic seizure or may enlarge our understanding of seizure dynamics. Further work is thus needed in order to shed more light on the functional mechanisms underlying seizure generation, spread, and termination.

6 Conclusion

We have investigated the Bayesian inference of time-dependent interaction properties, comparing it to the well-established evolution map approach [41] and the mean phase coherence [52] that yield estimators for the direction and the strength of interactions, respectively.

In the case of coupled, non-linear oscillators with time-independent interaction properties we observed limitations of the Bayesian inference method, where it was not able to improve shortcomings of other approaches, in particular with respect to inferring directed interactions between systems with structural differences. This could be shown both for two interacting Rössler oscillators with different natural frequencies, and for coupled Rössler and Lorenz oscillators, where the problem was even more manifest. Hence, Bayesian inference does not appear to widen the class of systems, where a phase-based description of interaction properties is meaningfully applicable. Furthermore, the canonical estimators $\hat{K}_{i\to j}$ for the strength of interactions miss a universal interpretation. It is not meaningful to compare the absolute values obtained for two different pairs of oscillators, as the coupling strengths alone contain only little information about the effect of the coupling without taking into account the dynamics of the individual oscillators themselves. Hence, only statements about the *evolution* of the strength of interaction between one pair of oscillators are meaningfully possible with the Bayesian framework. Of course, this limitation holds for many model-based characterizations of interaction properties (cf. [43,55,58–61,73,74]) and is not unique to the Bayesian approach.

Our investigations of temporal changes of interaction properties in the human brain during an epileptic seizure did not reveal transient changes of either the strength or direction of interactions that may give deeper insight into possible mechanisms underlying genesis, propagation and termination of seizures, but demonstrate that the use of Bayesian inference does allow inference of interaction properties with higher temporal resolution.

We have shown, that our proposed modification of the method for inferring time-varying interaction properties by partially forgetting prior knowledge is superior to the original method, in the sense that it achieves better goodness on average without the necessity of fine-tuning any parameter. When achieving better time resolution by reducing the window length, Bayesian inference and knowledge propagation in our modified algorithm allow improved accuracy compared to the original EMA method.

The Bayesian inference approach can easily be adapted to encompass network dynamics with any number L of partaking oscillators [42], although the number of required base functions and inferred coefficients scales with L^2 and limits the possible size of an investigated network. Still, it can be used to merge the benefits of Bayesian inference with those of triplet locking [75], which has been shown to yield better results than pairwise interaction estimation when dealing with large numbers of interacting systems.

In conclusion, in coupled systems where phase-based approaches are meaningful the investigated Bayesian inference method with our presented modification can improve the goodness of estimation of interaction properties at higher time resolution. However, we point out that the method in its current state cannot overcome difficulties of well-established methods when inferring non-linear, chaotic systems, particularly if they are structurally different. In such cases, the use of methods assessing structural differences might help to identify more adequate sets of basis functions.

J.W. acknowledges support by the Bonn-Cologne Graduate School of Physics and Astronomy. This work was supported by the Deutsche Forschungsgemeinschaft (Grant No. LE660/5-1). Both authors contributed equally to this paper.

References

1. C. Hugenii Huygens, *Horologium Oscillatorium* (Apud F. Muguet, Paris, 1673)
2. A.T. Winfree, J. Theor. Biol. **16**, 15 (1967)
3. Y. Kuramoto, *Chemical Oscillations, Waves and Turbulence* (Springer-Verlag, Berlin, 1984)
4. I.I. Blekhman, *Synchronization in Science and Technology* (ASME Press, 1988)
5. K.M. Weickmann, J. Geophys. Res. Oceans **96**, 3187 (1991)
6. A.S. Pikovsky, M.G. Rosenblum, J. Kurths, *Synchronization: A universal Concept in Nonlinear Sciences* (Cambridge University Press, Cambridge, 2001)
7. L. Glass, Nature **410**, 277 (2001)
8. A.K. Engel, P. Fries, W. Singer, Nat. Rev. Neurosci. **2**, 704 (2001)
9. F.J. Varela, J.P. Lachaux, E. Rodriguez, J. Martinerie, Nat. Rev. Neurosci. **2**, 229 (2001)
10. I.Z. Kiss, Y. Zhai, J.L. Hudson, Science **296**, 1676 (2002)
11. S.H. Strogatz, *Sync: the Emerging Science of Spontaneous Order* (Theia, New York, 2003)
12. A. Schnitzler, J. Gross, Nat. Rev. Neurosci. **6**, 285 (2005)
13. G. Buzsáki, *Rhythms of the Brain* (Oxford University Press, New York, 2006)
14. A. Arenas, A. Díaz-Guilera, J. Kurths, Y. Moreno, C. Zhou, Phys. Rep. **469**, 93 (2008)
15. S. Boccaletti, J. Kurths, G. Osipov, D.L. Valladares, C.S. Zhou, Phys. Rep. **366**, 1 (2002)
16. G.V. Osipov, J. Kurths, C. Zhou, *Synchronization in Oscillatory Networks,* Springer Series in Synergetics (Springer, Berlin, 2007)
17. K. Lehnertz, S. Bialonski, M.-T. Horstmann, D. Krug, A. Rothkegel, M. Staniek, T. Wagner, J. Neurosci. Methods **183**, 42 (2009)
18. J. Fell, N. Axmacher, Nat. Rev. Neurosci. **12**, 105 (2011)
19. M. Kapitaniak, K. Czolczynski, P. Perlikowski, A. Stefanski, T. Kapitaniak, Phys. Rep. **517**, 1 (2012)
20. J. Honerkamp, *Stochastic Dynamical Systems: Concepts, Numerical Methods, Data Analysis* (Wiley-VCH, New York, 1993)
21. H. Kantz, T. Schreiber, *Nonlinear Time Series Analysis*, 2nd edn. (Cambridge University Press, Cambridge, 2003)
22. N. Wiener, The theory of prediction, in *Modern Mathematics for Engineers*, edited by E.F. Beckenbach (McGraw-Hill, New York, 1956)
23. C.W.J. Granger, Econometrica **37**, 424 (1969)
24. E. Pereda, R. Quian Quiroga, J. Bhattacharya, Prog. Neurobiol. **77**, 1 (2005)
25. K. Hlaváčková-Schindler, M. Paluš, M. Vejmelka, J. Bhattacharya, Phys. Rep. **441**, 1 (2007)
26. J. Prusseit, K. Lehnertz, Phys. Rev. E **77**, 041914 (2008)

27. M.C. Romano, M. Thiel, J. Kurths, C. Grebogi, Phys. Rev. E **76**, 036211 (2007)
28. R.G. Andrzejak, A. Ledberg, G. Deco, New J. Phys. **8**, 6 (2006)
29. K. Ishiguro, N. Otsu, M. Lungarella, Y. Kuniyoshi, Phys. Rev. E **77**, 026216 (2008)
30. S. Łeski, D.K. Wójcik, Phys. Rev. E **78**, 41918 (2008)
31. M. Martini, T.A. Kranz, T. Wagner, K. Lehnertz, Phys. Rev. E **83**, 011919 (2011)
32. T. Wagner, J. Fell, K. Lehnertz, New J. Phys. **12**, 053031 (2010)
33. T. Wagner, N. Axmacher, K. Lehnertz, C.E. Elger, J. Fell, Cortex **46**, 256 (2010)
34. K. Lehnertz, Physiol. Meas. **32**, 1715 (2011)
35. T. Stankovski, A. Duggento, P.V.E. McClintock, A. Stefanovska, Phys. Rev. Lett. **109**, 024101 (2012)
36. M.G. Rosenblum, A.S. Pikovsky, J. Kurths, C. Schaefer, P.A. Tass, Phase synchronization: from theory to data analysis, in *Handbook of Biological Physics*, edited by F. Moss, S. Gielen, (Elsevier Science, Amsterdam, 2001), pp. 297–321
37. J.O. Berger, *Statistical Decision Theory and Bayesian Analysis* (Springer, Berlin, 1985)
38. J. Guckenheimer, J. Math. Biol. **1**, 259 (1975)
39. A.T. Winfree, *The Geometry of Biological Time* (Springer-Verlag, New York, 1980)
40. M.G. Rosenblum, A.S. Pikovsky, J. Kurths, Phys. Rev. Lett. **76**, 1804 (1996)
41. M.G. Rosenblum, A.S. Pikovsky, Phys. Rev. E **64**, 045202 (2001)
42. A. Duggento, T. Stankovski, P.V.E. McClintock, A. Stefanovska, Phys. Rev. E **86**, 061126 (2012)
43. D.A. Smirnov, B.P. Bezruchko, Phys. Rev. E **68**, 046209 (2003)
44. D.A. Smirnov, R.G. Andrzejak, Phys. Rev. E **61**, 036207 (2005)
45. D. Smirnov, B. Schelter, M. Winterhalder, J. Timmer, Chaos **17**, 013111 (2007)
46. V.N. Smelyanskiy, D.G. Luchinsky, A. Stefanovska, P.V.E. McClintock, Phys. Rev. Lett. **94**, 098101 (2005)
47. D.G. Luchinsky, M.M. Millonas, V.N. Smelyanskiy, A. Pershakova, A. Stefanovska, P.V.E. McClintock, Phys. Rev. E **72**, 021905 (2005)
48. A. Bandrivskyy, D.G. Luchinsky, P.V.E. McClintock, V.N. Smelyanskiy, A. Stefanovska, Stochastics and Dynamics **05**, 321 (2005)
49. A. Duggento, D.G. Luchinsky, V.N. Smelyanskiy, I. Khovanov, P.V.E. McClintock, Phys. Rev. E **77**, 061106 (2008)
50. A. Duggento, D.G. Luchinsky, V.N. Smelyanskiy, P.V.E. McClintock, J. Stat. Mech. Theor. Exp. **2009**, P01025 (2009)
51. D.G. Luchinsky, V.N. Smelyanskiy, M. Millonas, P.V.E. McClintock, Eur. Phys. J. B **65**, 369 (2008)
52. F. Mormann, K. Lehnertz, P. David, C.E. Elger, Physica D **144**, 358 (2000)
53. O.E. Rössler, Phys. Lett. A **57**, 397 (1976)
54. E.N. Lorenz, J. Atmos. Sci. **20**, 130 (1963)
55. S. Porz, M. Kiel, K. Lehnertz, Chaos **24**, 033112 (2014)
56. A. Rothkegel, K. Lehnertz, Chaos **22**, 013125 (2012)
57. B. Boashash, *Time frequency signal analysis: methods and applications* (Longman Cheshire, Melbourne, 1992)
58. R. Quian Quiroga, J. Arnhold, P. Grassberger, Phys. Rev. E **61**, 5142 (2000)
59. G. Nolte, O. Bai, L. Wheaton, Z. Mari, S. Vorbach, M. Hallett, Clin. Neurophysiol. **115**, 2292 (2004)
60. H. Osterhage, F. Mormann, T. Wagner, K. Lehnertz, Int. J. Neural. Syst. **17**, 139 (2007)
61. D. Chicharro, R.G. Andrzejak, Phys. Rev. E **80**, 026217 (2009)
62. P.J. Franaszczuk, G.K. Bergey, P.J. Durka, H.M. Eisenberg, Electroencephalogr. Clin. Neurophysiol. **106**, 513 (1998)
63. S.J. Schiff, D. Colella, G.M. Jacyna, E. Hughes, J.W. Creekmore, A. Marshall, M. Bozek-Kuzmicki, G. Benke, W.D. Gaillard, J. Conry, S.R. Weinstein, Clin. Neurophysiol. **111**, 953 (2000)
64. C.C. Jouny, P.J. Franaszczuk, G.K. Bergey, Clin. Neurophysiol. **114**, 426 (2003)
65. S. Bialonski, K. Lehnertz, Chaos **23**, 033139 (2013)
66. P.J. Franaszczuk, G.K. Bergey, M.J. Kaminski, Electroencephalogr. Clin. Neurophysiol. **91**, 413 (1994)
67. M. Le Van Quyen, C. Adam, M. Baulac, J. Martinerie, F.J. Varela, Brain Res. **792**, 24 (1998)
68. J. Arnhold, P. Grassberger, K. Lehnertz, C.E. Elger, Physica D **134**, 419 (1999)
69. M. Chavez, J. Martinerie, M. Le Van Quyen, J. Neurosci. Methods **124**, 113 (2003)
70. M. Staniek, K. Lehnertz, Biomed. Tech. **54**, 323 (2009)
71. F. Wendling, F. Bartolomei, L. Senhadji, Phil. Trans. Roy. Soc. A **367**, 297 (2009)
72. K. Lehnertz, G. Ansmann, S. Bialonski, H. Dickten, C. Geier, S. Porz, Physica D **267**, 7 (2014)
73. L. Faes, G. Nollo, A. Porta, Phys. Rev. E **83**, 051112 (2011)
74. J. Runge, J. Heitzig, N. Marwan, J. Kurths, Phys. Rev. E **86**, 061121 (2012)
75. B. Kralemann, A. Pikovsky, M. Rosenblum, New J. Phys. **16**, 085013 (2014)